



# An experimental investigation on the performance of a flat-plate solar collector using eco-friendly treated graphene nanoplatelets–water nanofluids

Naveed Akram<sup>1,2</sup> · Rad Sadri<sup>1</sup> · S. N. Kazi<sup>1</sup> · S. M. Ahmed<sup>1</sup> · M. N. M. Zubir<sup>1</sup> · Mohd Ridha<sup>1,3</sup> · Manzoore Soudagar<sup>1</sup> · Waqar Ahmed<sup>1</sup> · Mazdak Arzpeyma<sup>1</sup> · Goh Boon Tong<sup>4</sup>

Received: 13 January 2019 / Accepted: 19 February 2019 / Published online: 7 March 2019

© Akadémiai Kiadó, Budapest, Hungary 2019

## Abstract

The research on the use of nanofluids in thermal energy devices, like solar collectors, has secured a high place in the scientific community of recent years. In the present study, the effects of clove-treated graphene nanoplatelet nanofluids on the performance of flat-plate solar collector were investigated. For this, the graphene nanoplatelets and clove buds were covalently functionalized using the one-pot technique. Zeta potential test was conducted to check the stability of the graphene nanoplatelets–water nanofluid and found highly stable for 45 days. In the next step, three different mass concentrations 0.025 mass%, 0.075 mass% and 0.1 mass% were synthesized. The thermal performance of flat-plate solar collector at these three concentrations of the nanofluids of three different mass flow rates 0.0133, 0.0200 and 0.0260 kg s<sup>-1</sup> m<sup>-2</sup> was investigated in the next step. The results revealed that the thermal performance of solar collector enhances with the increase in mass concentration and mass flow rates and decreases with an increase in reduced temperature parameter. The highest thermal performance of a solar collector has reached 78% at mass concentration 0.1 mass% and flow rate 0.0260 kg s<sup>-1</sup> m<sup>-2</sup> which is 18.2% higher than water at the same flow rate conditions.

**Keywords** Thermal performance · Heat transfer · Flat-plate solar collector · Graphene nanofluids · Efficiency · Green synthesis

## List of symbols

$A_c$	Collector area (m <sup>2</sup> )	GNP	Graphene nanoplatelet
$C_p$	Specific heat of fluid (J kg <sup>-1</sup> K <sup>-1</sup> )	$G_T$	Incident solar radiation (W m <sup>-2</sup> )
CGNP	Clove-treated graphene nanoplatelet	$k$	Thermal conductivity (W m <sup>-1</sup> K <sup>-1</sup> )
CTAB	Cetyltrimethylammonium bromide	$\dot{m}$	Mass flow rate (kg s <sup>-1</sup> m <sup>-2</sup> )
EG	Ethylene glycol	MWCNT	Multi-walled carbon nanotubes
FPSC	Flat-plate solar collector	PEG 400	Polyethylene glycol 400
$F_R$	Heat removal factor	PVD	Physical vapor deposition
		$Q_u$	Useful energy gain
		$R^2$	Root mean square error

✉ Naveed Akram  
naveed.me@must.edu.pk

✉ Rad Sadri  
rod.sadri@gmail.com

✉ S. N. Kazi  
salimnewaz@um.edu.my

<sup>1</sup> Faculty of Mechanical Engineering, University of Malaya, 50603 Kuala Lumpur, Malaysia

<sup>2</sup> Department of Mechanical Engineering, Mirpur University of Science and Technology (MUST), Mirpur, AJK 10250, Pakistan

<sup>3</sup> Faculty of Engineering, Centre of Advanced Manufacturing and Material Processing (AMMP), University of Malaya, 50603 Kuala Lumpur, Malaysia

<sup>4</sup> Department of Physics, Faculty of Science, Low Dimensional Materials Research Centre, University of Malaya, 50603 Kuala Lumpur, Malaysia

SDBS	Sodium dodecyl benzene sulfonate
SDS	Sodium dodecyl sulfate
$T_a$	Ambient temperature (K)
$T_i$	Inlet fluid temperature (K)
$T_o$	Outlet fluid temperature (K)
$U_L$	Total heat loss

### Greek symbol

$\alpha$	Absorptance of the absorber plate
$\rho$	Density of fluid ( $\text{kg m}^{-3}$ )
$\tau$	Transmittance of the glass cover
$\eta_c$	Collector efficiency
$\mu$	Dynamic viscosity (Pa s)
$\varphi$	Mass fraction

### Subscripts

bf	Base fluid
nf	Nanofluid
np	Nanoparticles

## Introduction

The population and energy demand of the world are increasing dramatically. Industrialization and globalization of the present human societies are the main reasons for this enhancement in the energy demands. According to the International Energy Agency [1], the global energy demand will grow 30% at the end of 2040. At present, 86% of total energy demands are fulfilled with fossil fuel [2]. The fossil fuel resources are declining fast, the environment is getting polluted, and climate change is becoming the main global problem. This is enforcing human to think of other energy resources [3]. The unlimited, cheapest and cleanest source of energy is solar thermal energy which is abundantly available everywhere on earth surface. Solar energy is considering the best alternative source for fossil fuels. There are several devices for harvesting solar energy; solar collectors are the most common devices for receiving solar radiation and converting it into useful heat gain [4]. Flat-plate solar collectors are the most popular type of solar collectors for commercial and residential applications. The efficiency and outlet temperature of FPSC are comparatively low. The effectiveness of FPSC depends on many factors such as materials, design [5], angle [6], climate condition [7] and working fluid [8]. Besides the other methods to increase the performance of collectors, the most effective one is to replace the working fluid with a high convective heat transfer coefficient fluid [9]. A working fluid with low heat capacity and high thermal conductivity can enhance the heat transfer rate from the collector's absorber plate to working fluid and enhance outlet

temperature of the collector fluid. The thermal efficiency of FPSC can be enhanced by using a new generation of working fluid, i.e., nanofluids which contain high thermal conductivity than conventional working fluid [10]. Nanofluids are prepared by dispersing of nanometric size (1–100 nm) solid particles in a base fluid (DI water, oil, brines, propylene glycol, etc.) [11–13]. The term of nanofluids was first discovered by Choi [14]. Masuda et al. [15] were the first who noticed the huge change in thermophysical properties of base liquid after the dispersion of nanoparticles. Table 1 elucidates brief experimental studies of the performance of FPSC using various nanofluids. From the literature, it is noticed that most of the researchers use metal or metal oxides as base nanoparticles for experimental studies on flat-plate solar collectors [16]. However, few of them [17, 18] report data with carbon nanostructure. Vakili et al. [19] investigated the outcome of GNPs base nanofluid for the domestic hot water system. They found that with increase in mass concentration and mass flow rate the performance of solar collectors was improved. The maximum zero loss efficiency is 93.24%, whereas this efficiency for base fluid is 70% at same conditions. However, no data were conveyed about the stability of nanofluid. Ahmadi et al. [20] used a high concentration of GNPs nanofluid to evaluate the thermal performance of FPSC. They also checked the effect of pH on stability and considered pH 11.3 as the best for their study. The thermal conductivity of nanofluid was increased 13% in comparison with that of water. On the other hand, it enhances 18.8% the performance of a FPSC compared to water alone as the working fluid.

In most recent studies, Verma et al. [38] reported the performance of FPSC using MWCNT, GNPs, CuO, Al<sub>2</sub>O<sub>3</sub>, TiO<sub>2</sub> and SiO<sub>2</sub>. They found that with GNPs the thermal performance of collector enhanced 16.97% while this value was 23.47% for MWCNT. From all nanofluids used in this study, GNPs have minimum pumping power loss.

The stability of nanofluids is very important for enhancement in the effectiveness of FPSC. The outstanding properties of nanofluids cannot be attained by simply mixing a base fluid with nanoparticles. Despite the high specific surface area of graphene, it has tendency to agglomerate due to the strong  $\pi$ - $\pi$  stacking interactions. In addition, the dispersibility of graphene in aqueous media is one of the most critical parameters in heat transfer systems. Thus, different techniques (both physical and chemical routes) have been proposed to enhance the dispersibility of graphene in aqueous media [39]. In general, these techniques involve non-covalent and covalent functionalization of graphene. Covalent functionalization is typically used to attain high dispersion of carbon nanomaterials in aqueous media [40, 41].

**Table 1** Experimental studies on flat-plate solar collector using nanofluids

Researcher	Surfactant	Base fluid	Nanoparticles			Remarks
			Type	Size (nm)	Volume or mass fraction	
Natarajan and Sathish [9]	SDS	H <sub>2</sub> O	MWCNT	N/A	0.2– 1.0 vol%	Thermal conductivity is 41% at 1% concentration
Polvongsri and Kiatsiriroat [21]	N/A	H <sub>2</sub> O	Ag (Silver)	20	0.1 and 1.0 mass%	Nanofluids are suitable at high temperature and high mass flow rate
Yousefi et al. [22]	Triton X-100	H <sub>2</sub> O	Al <sub>2</sub> O <sub>3</sub>	15	0.2 and 0.4 mass%	28.3% increment in efficiency of FPSCs at 0.2 mass% nanoparticles
Yousefi et al. [17]	Triton X-100	H <sub>2</sub> O	MWCNT	10–30	0.2 and 0.4 mass%	The efficiency of the FPSC was found maximum at 0.4 mass% concentration and 0.05 kg s <sup>-1</sup> flow rate
Vijayakumar et al. [18]	Polysorbate 80	H <sub>2</sub> O	CNT	1	0.40,0.50 and 0.60 mass%	At 0.5% concentration, improvement in efficiency is 39%
Jamal-Abad et al. [23]	SDS	H <sub>2</sub> O	Cu	35	0.05 and 0.1 mass%	Increment in efficiency is 24% for 0.05 mass% nanofluids
Said et al. [24]	Without	H <sub>2</sub> O-EG and water	Al <sub>2</sub> O <sub>3</sub>	13	0.05–0.1 vol%	Water-Al <sub>2</sub> O <sub>3</sub> is more stable than Al <sub>2</sub> O <sub>3</sub> / water-EG Thermal conductivity increases with an increase in concentration
Noghrehbadi et al. [25]	Without	H <sub>2</sub> O	SiO <sub>2</sub>	12	1 mass%	Efficiency increases by using nanofluid compared to water
Verma et al. [26]	CTAB	H <sub>2</sub> O	MgO	40	0.25 to 1.5 vol%	The efficiency of the collector is increased 9.34% at 0.75 vol% and 1.5 lpm
Vincely and Natarajan [27]	Without	DI water	GO	N/A	0.005,0.01 and 0.02 mass%	Efficiency of collector is enhanced with 7.3% at 0.02 mass% and 0.0167 kg s <sup>-1</sup>
Said et al. [28]	N/A	H <sub>2</sub> O	Al <sub>2</sub> O <sub>3</sub>	13	0.1 and 0.3 vol%	Energy efficiency is enhanced by 83.5% at 0.3 vol% and 1.5 kg/min Thermal efficiency is 50% more than the existing system
Kim et al. [29]	Without	H <sub>2</sub> O	Al <sub>2</sub> O <sub>3</sub>	20 to 50	0.5,1.0 and 1.5 vol%	The highest efficiency improvement is 24.1%
Jouybari et al. [30]	Without	H <sub>2</sub> O	SiO <sub>2</sub>	20 to 30	0.2,0.4 and 0.6 vol%	Thermal efficiency is improved by 8.1% by using nanofluid
Sharafeldin et al. [31]	Without	H <sub>2</sub> O	WO <sub>3</sub>	90	0.0167,0.0333 and 0.0666 vol%	Maximum efficiency enhancement is 71.87% at 0.0066 vol% and 0.0195 kg s <sup>-1</sup> The maximum enhanced in absorbed energy parameter is 13.48%
Kang et al. [32]	N/A	H <sub>2</sub> O	Al <sub>2</sub> O <sub>3</sub>	20,50 and 100	0.5,1.0 and 1.5	The maximum efficiency of FPSC is 74.9% at 1.0 vol% and 20 nm particle size; it is 14.8% improved as compared to water
Stalin et al. [33]	N/A	H <sub>2</sub> O	CeO <sub>2</sub>	25	0.01 vol%	The maximum efficiency is 78.2% which is 21.5% higher as compared to water
Sundar et al. [34]	SDBS	H <sub>2</sub> O	Al <sub>2</sub> O <sub>3</sub>	< 20	0.1 and 0.3 vol%	Collector effectiveness for 0.086 kg s <sup>-1</sup> is increased by 22% and 52.80% with 0.3 vol% concentration
Sharafeldin and Gróf [35]	Without	H <sub>2</sub> O	CeO <sub>2</sub>	25	0.0167,0.033 and 0.066 vol%	The optimum flow rate for the study is 0.033 vol% at which efficiency improvement is 10.74%
Farajzadeh et al. [36]	CTAB	H <sub>2</sub> O	Al <sub>2</sub> O <sub>3</sub> TiO <sub>2</sub>	20 and 15	0.1 mass%	The thermal efficiency of the mixture of nanoparticles is 26%, which is higher than individual particles and water
Mirzaei et al. [37]	Without	H <sub>2</sub> O	Al <sub>2</sub> O <sub>3</sub>	20	0.1 vol%	Maximum efficiency of collector 23.6% can achieve at 2 lpm

The above-mentioned studies based on the latest reviews [42–44] on the topic show that no research had been done on the application of bio-based synthesis of covalently functionalized graphene nanoplatelet nanofluid on the performance of flat-plate solar collector although clove-treated GNPs (CGNPs) had good thermophysical properties and stability which was found earlier [39]. The focus of the current study is on the performance of FPSC, using CGNP–water nanofluid as a working fluid. Also, the environmental factors such as solar radiation (heat flux) and ambient temperature on the thermal performance of collector, effect of three different mass concentrations of nanofluid, three mass flow rates and the optimal flow rate were also taken under consideration for investigation.

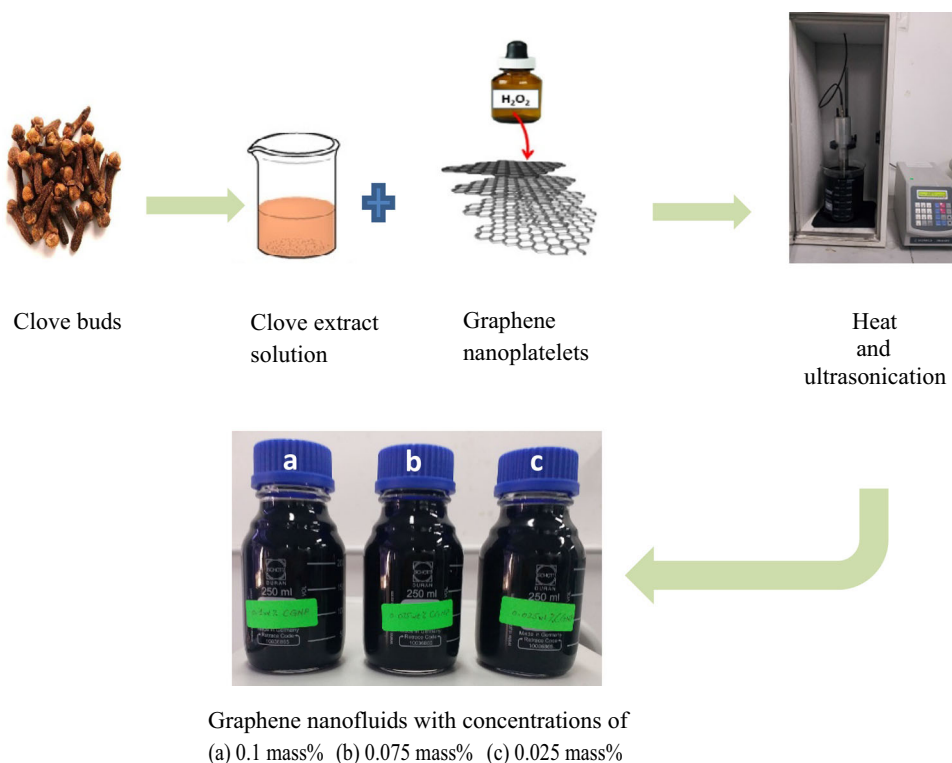
## Experimental

There are four subsections presented in this section: The initial part describes the preparation of CGNP–water nanofluid, the second part describes the experimental setup of FPSC, third part provides details about the testing method, and the final part of this unit describes the uncertainty analysis.

## Synthesis of nanofluids

In this investigation, the working fluid used is the DI water and water-based CGNPs nanofluids. The pristine GNPs (supplier: XG Sciences, USA) specific surface area  $750 \text{ m}^2 \text{ g}^{-1}$ , thickness 2 nanometers, lateral size 2 nm and purity 99.5% hydrogen peroxide ( $\text{H}_2\text{O}_2$ , 30%) (supplier: Sigma-Aldrich (M) Sdn. Bhd.) and dried clove buds (from a grocery store in Kuala Lumpur, Malaysia) were used for covalent functionalization of GNPs. The GNPs are functionalized by following the procedure of previous researchers [39]. The preparation of nanofluid was conducted in a two-step method. The clove-treated GNPs (CGNPs) were dispersed into DI water by using ultrasonication probe (Sonic Vibra Cell, VC 750, Sonic & Materials, Inc., USA) continuously for 60 min. The synthesis of nanofluids had carried out at three different particle concentrations containing 0.025, 0.075 and 0.1 mass% as shown in Fig. 1. Zeta potential analyzer was used for testing the stability of nanofluids. Figure 2 shows the measured zeta potential values as a function of pH for the CGNP aqueous suspension. It can be observed that the CGNP nanofluid has high negative values ( $-4.42 \text{ mV}$  to  $-49.5 \text{ mV}$ ) within the pH variations from 1.84 to 10.55. More importantly, the zeta potential values for the CGNP nanofluids are far from the isoelectric point (i.e., point of zero charge), which indicates that this pH range (2.8–10.55) results in strong electric repulsion forces

**Fig. 1** Preparation of graphene nanofluids



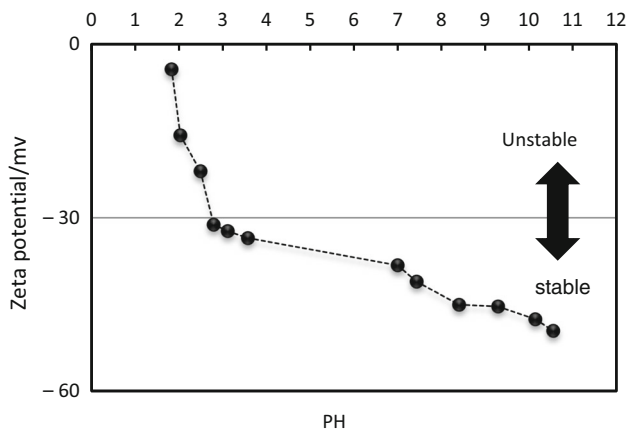


Fig. 2 Zeta potential values of CGNPs nanofluid at a different pH

between the particles of CGNPs. This prevents aggregation of the CGNPs by non-covalent interactions such as  $\pi$ - $\pi$  interactions. CGNP-water nanofluids found stable for 45 days.

### Experimental setup

To investigate the thermal performance of FPSC, the experimentations were conducted in the laboratory (indoor testing) in the Department of Mechanical Engineering at the University of Malaya, Kuala Lumpur, Malaysia. The specifications of the solar collector used in this study are given in Table 2. Schematic diagram of the test rig layout and photograph of the setup are shown in Figs. 3 and 4, respectively.

A centrifugal electric pump (Araki EX-30R) was used for forced circulation of working fluid. A tank having capacity 8 L was used as a nanofluid reservoir, and the flow rate was measured using a digital flow meter (SE32-PV). To control the flow rate during experiments, a needle valve was installed before the flow meter, and to measure the inlet and outlet temperatures of solar collector, calibrated PT-100 resistance temperature detectors (RTDs) were used. A T-type self-adhesive thermocouple was used for ambient temperature measurement while constant heat flux analogous to that of solar radiation at the surface of the collector was arranged with the help of flexible adhesive heater. The nanofluid temperature at the inlet of the collector was controlled by a refrigerated water bath circulator with jacket tank.

### Testing method

The ASHRAE Standard 93-2003 [45] was used for indoor testing, to evaluate the effectiveness of FPSC. This standard is introduced for outdoor as well as indoor testing of the collector using single-phase fluid as shown in Fig. 5. According to

ASHRAE standard 93-2003 [45], the flow rates were varied from 0.8 to 1.6 L min<sup>-1</sup> m<sup>-2</sup>. The inlet temperature was in tune between 30 and 65 °C. The ambient temperature for all data periods must be less than 30 °C. The angle of solar collector was adjusted between 30 and 60 degrees. The minimum heat flux at the surface of collector received from radiation was 790 W m<sup>-2</sup>. As ASHRAE Standard 93-2003 was followed, so the flow rates used in this study were 0.0133, 0.0200 and 0.0260 kg s<sup>-1</sup> m<sup>-2</sup>. The inlet temperature was in the range of 30, 40 and 50 °C. All the experiments were conducted at steady-state conditions and different heat flux rates analogous to the solar radiations to find out the thermal efficiency of FPSC. The ratio between useful heat gain  $Q_u$  and total energy received by absorber plate provides the effectiveness of collector and is calculated using Eq. (1) [46].

$$\eta_c = \frac{Q_u}{A_c G_T} \tag{1}$$

Equation (2) is used to calculate the useful heat gain energy, and it is calibrated by taking the difference between heat energy absorbed and heat energy loss by absorber plate as given in Eq. (3).

$$Q_u = \dot{m} C_p (T_o - T_i) = \rho V C_p (T_o - T_i) \tag{2}$$

The collector efficiency can be calculated by using Eq. (4) or Eq. (5)

$$Q_u = A_c F_R [G_T (\tau\alpha) - U_L (T_i - T_a)] \tag{3}$$

$$\eta_c = \frac{\rho V C_p (T_o - T_i)}{A_c G_T} \tag{4}$$

$$\eta_c = \frac{A_c F_R [G_T (\tau\alpha) - U_L (T_i - T_a)]}{A_c G_T} \tag{5}$$

Equation (5) can be rewritten as shown in Eq. (6) where  $F_R$  is known as heat removal factor according to Hottel-Whillier equation, as given in Eq. (7).

$$\eta_c = F_R (\tau\alpha) - F_R U_L \left( \frac{T_i - T_a}{G_T} \right) \tag{6}$$

$$F_R = \frac{\dot{m} C_p (T_o - T_i)}{A_c [G_T (\tau\alpha) - U_L (T_i - T_a)]} \tag{7}$$

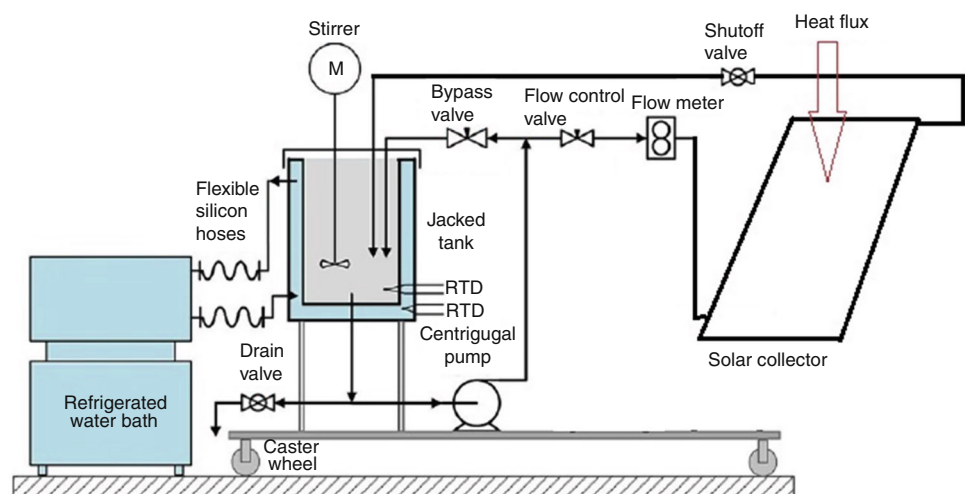
In Eq. 7,  $\dot{m}$  is the mass flow rate,  $T_i$  is the collector inlet temperature,  $T_o$  is the collector outlet temperature, and  $T_a$  is represented as the ambient temperature.  $G_T, A_c, \tau\alpha$  and  $U_L$  are represented as solar radiation, the area of the collector, absorption-transmittance product and overall all heat losses, respectively, while  $C_p$  is specific heat of operational fluid. The specific heat and density of nanofluids are measured by Eqs. (8) and (9) [47–49].

$$(\rho C_p)_{nf} = (\rho C_p)_{nf}(\phi) + (\rho C_p)_{bf}(1 - \phi) \tag{8}$$

$$\rho_{nf} = \rho_{np}(\phi) + \rho_{bf}(1 - \phi) \tag{9}$$

**Table 2** Specifications of FPSC used in this investigation

Specification	Dimension	Unit
Length	1135	mm
Width	600	mm
Depth	90	mm
Collector occupied area	0.6810	m <sup>2</sup>
Absorber area	0.4645	m <sup>2</sup>
Glass thickness	5	mm
Riser tube outer diameter (do)	12.7	mm
Riser tube inner diameter (di)	11.6	mm
Header tube outer diameter (Do)	22.2	mm
Header tube inner diameter (Di)	20.9	mm
Center distance between tubes	128	mm
The emissivity of the glass cover	0.88	(dimensionless)
Absorber absorption coefficient	0.95	(dimensionless)
Back insulation	50	mm
The thermal conductivity of the insulation	0.04	W/mK
Transmittance-absorptance product	0.8772	
Tilt angle	30°	

**Fig. 3** Schematic diagram of the test rig

Thermal conductivity can be evaluated by using Eq. (10) [49].

$$k_{nf} = k_{bf} \frac{k_{np} + (n-1)k_{bf} - (n-1)\varphi(k_{bf} - k_{np})}{k_{np} + (n-1)k_{bf} - \varphi(k_{bf} - k_{np})} \quad (10)$$

Thermophysical properties of nanofluids play an important role to increase the performance of solar collectors [50]. The thermophysical properties (thermal conductivity, dynamic viscosity and specific heat capacity) of CGNPs are presented in Table 3. The solar collector's thermal efficiency  $\eta_c$  is considered to plot a graph using Eq. (6) against reduced temperature parameter  $\left(\frac{T_i - T_a}{G_T}\right)$ , providing a straight line. This straight line intersects the

thermal efficiency line (vertical axis line) at  $F_R(\tau\alpha)$ . At this point, the inlet temperature of collector equal to the ambient temperature and the thermal efficiency of the collector reach its highest value. This point is also known as zero loss efficiency point. On the other side, the thermal efficiency is zero when the straight line intersects horizontal axis (reduced temperature line). The parameter  $F_R(\tau\alpha)$  is known as absorbed energy parameter, and  $F_R U_L$  is known as removed energy parameter.

### Uncertainty analysis

In any experimental investigation, the collected data have few errors and inaccuracies which cannot be avoided,



Fig. 4 Photograph of the setup

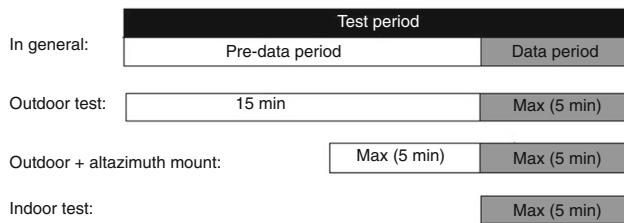


Fig. 5 Test and the pre-data period for calculating the efficiency of FPSC

which create an uncertainty in the experimental data. Hence, in this investigation, the accuracy of thermal efficiency for flat-plate solar collector is calibrated from the collected experimental data and it was calculated using uncertainty analysis. The efficiency of flat-plate solar collector used in this study can be conveyed in a proportional form as:

$$\eta_c \propto \frac{\text{Actual useful energy collected}}{\text{heat flux received at the surface of collector}} \propto \frac{\rho VC_p(T_o - T_i)}{G_T} \tag{11}$$

$$\Rightarrow \eta_c \propto \rho VC_p G_T^{-1} (T_o - T_i) \propto \rho VC_p G_T^{-1} \Delta T \tag{12}$$

The uncertainty ( $\omega$ ) in the value of R can be expressed using the following relation (Holman [51] and Kline and McClintock [52]), as shown in Eq. (13).

$$\frac{\omega_R}{R} = \left[ \sum_{i=1}^n \left( \frac{a_i \omega_{x_i}}{x_i} \right)^2 \right]^{0.5} \tag{13}$$

Consequently, using Eq. (12), the experimental data are used to find the uncertainty in the value of FPSC's efficiency using the following relation, as given in Eq. (14):

$$\frac{\omega_{\eta_c}}{\eta_c} = \left[ \left( \frac{\omega_{\rho}}{\rho} \right)^2 + \left( \frac{\omega_V}{V} \right)^2 + \left( \frac{\omega_{C_p}}{c_p} \right)^2 + \left( \frac{\omega_{G_T}}{G_T} \right)^2 + \left( \frac{\omega_{\Delta T}}{\Delta T} \right)^2 \right]^{0.5} \tag{14}$$

Table 3 Thermophysical properties (specific heat, thermal conductivity, dynamic viscosity and density) of CGNPs at various mass fractions

Thermal property				
Concentration of nanoparticles/%	Specific heat/J kg <sup>-1</sup> K <sup>-1</sup>	Viscosity/mPa s	Thermal conductivity/W m <sup>-1</sup> K <sup>-1</sup>	Density/kg m <sup>-3</sup>
Water	4142	0.829	0.611	995.50
0.025%	4123	0.844	0.636	995.60
0.075%	4096	0.868	0.681	995.80
0.1%	4080	0.885	0.708	995.90

The uncertainty values of the five independent variables are 0.04%, 1.67%, 2.75%, 1.75% and 0.67%, respectively. Hence, the uncertainty in the measured efficiency of the FPSC was estimated to be 3.75%. The maximum variation in ambient temperature, inlet temperature and radioactive flux in each test period was  $\pm 0.5$  °C,  $\pm 0.1$  °C, and  $\pm 25$  W m<sup>-2</sup>, respectively.

## Results and discussions

The enhancement in thermophysical properties of CGNP–water nanofluid as shown in Table 3 was examined and comprehensively discussed in this section. The results presented in this section are divided into two parts: In the first part of study DI water and in the second part of study CGNP nanofluids were presented. After that, a comparison of DI water and nanofluids results was presented at a different mass flow rate. As the concentration of nanoparticle has a remarkable effect on thermophysical properties, three different mass concentrations (0.025, 0.075 and 0.1 mass%) were used in this study.

### Water as working fluid in FPSC

The experiments were carried out in the department of mechanical engineering at the University of Malaya, Malaysia, at a time interval of 9:00 to 16:00 h. All the experiments performed by following the ASHRAE Standard 93-2003 for indoor testing and DI water were initially used as the working fluid to check the accuracy, repeatability and validity of the recorded data. All the test runs were performed several times at different flow rates of 0.0133, 0.0200 and 0.026 kg s<sup>-1</sup> m<sup>-2</sup>, and the best data were chosen for presentation. The heat absorbed parameter  $F_R(\tau\alpha)$ , heat removed parameter  $F_R U_L$  and thermal efficiency of flat-plate solar collector against reduced temperature parameter for DI water are shown in Table 4 and Fig. 6. From Table 4, it is clearly shown that the value of  $F_R(\tau\alpha)$  and  $F_R U_L$  increases as mass flow rate increases from 0.0133 to 0.0260 kg s<sup>-1</sup> m<sup>-2</sup> so the thermal efficiency also increases with mass flow rate. All the data presented in Fig. 6 are based on the fitted linear equation, and  $R^2$  represents the root mean square error for these data points, which reflect that how close the data points are to the trend line.

### CGNP nanofluid as working fluid in FPSC

The values of  $F_R(\tau\alpha)$  and  $F_R U_L$  for CGNP and water at different mass flow rates and mass concentrations are presented in Table 5. The results arranged in this table are

**Table 4** Heat absorbed factor and heat removal factor at a different flow rate for DI water

Mass flow rate/kg s <sup>-1</sup> m <sup>-2</sup>	$F_R(\tau\alpha)$	$F_R U_L$	$R^2$
0.0133	0.6120	4.8261	0.9684
0.0200	0.6640	5.2561	0.9773
0.0260	0.6829	5.2945	0.9739

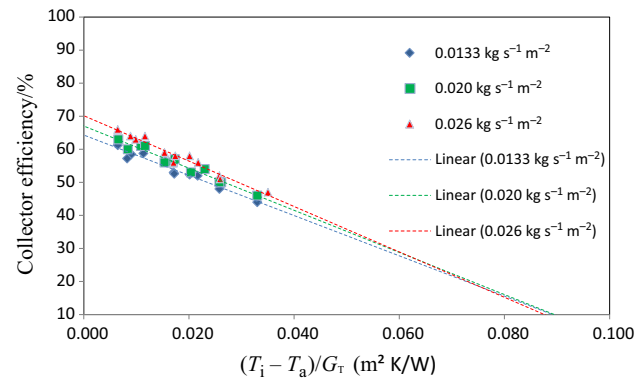


**Fig. 6** Efficiency of FPSC using DI water

based on the mass flow rate. It showed that the values of heat removal factor for nanofluids were higher than those of water and it goes on increasing as the flow rate increases. Table 3 shows that the thermal conductivity of nanofluid is higher than water data. So, based on the results of data from Tables 3 and 5, the convective heat transfer coefficient was higher for CGNP than that for water alone. Therefore, the thermal performance of solar collector could be enhanced by using CGNP/water nanofluid.

The efficiency of solar collector is enhanced due to the convective heat transfer coefficient, and this value is directly related to the thermal conductivity of the heat transfer liquid or nanofluid used. The significant enhancement in convective heat transfer coefficient is mainly due to the thin thermal boundary layer formed at the riser tube walls resulting from the thermal conductivity enhancement of CGNP/water nanofluid as well as a decrease in thermal resistance between the nanofluid and inner wall surface of the riser tube. In addition, carbon nanomaterials such as graphene and CNTs result in thinner thermal boundary layer thickness. The specific surface area and Brownian motion of the nanoparticles also play a role in influencing the convective heat transfer coefficient [11]. It can be observed that there is an increment in the convective heat transfer coefficient when the  $Re$  is increased for the CGNP–water nanofluids and DI water. Moreover, the concentration of nanoparticles has a pronounced effect on the convective heat transfer coefficient of the CGNP–water



**Table 5** Heat absorbed and heat removal factor of CGNP on the same flow rate

Mass flow rate/kg s <sup>-1</sup> m <sup>-2</sup>	Mass concentration/mass%	F <sub>R</sub> (τ $\alpha$ )	F <sub>R</sub> U <sub>L</sub>	R <sup>2</sup>
0.0133	0.1	0.7437	6.0120	0.9918
	0.075	0.7324	5.5838	0.9714
	0.025	0.6452	5.4250	0.9779
	DI water	0.6120	4.8261	0.9684
0.0200	0.1	0.8135	6.4032	0.9758
	0.075	0.7873	6.2325	0.9784
	0.025	0.6929	5.9928	0.9860
	DI water	0.6640	5.2561	0.9773
0.0260	0.1	0.8230	7.0131	0.9831
	0.075	0.8196	6.6232	0.9573
	0.025	0.7057	6.1816	0.9737
	DI water	0.6729	5.2945	0.9739

nanocoolants. We attribute this effect to the reduced thermal boundary layer thickness as well as the increased thermal conductivity in the presence of water-based CGNP nanocoolants. Furthermore, we believe that other factors such as the specific surface area and Brownian motion of the CGNPs play a key role in the convective heat transfer coefficient. Several researchers gave reasons in the previous works [53, 54]. Another factor that increases Brownian motion is forced circulation which was implemented by the pump. The pump supplies energy to the operating working fluid. Due to this energy collision between liquid molecules and the solid particles, it improved convective heat transfer coefficient and later thermal performance of the solar collector. Another factor that affects the thermal performance is the reduced temperature parameter. Figure 8a–c shows the efficiency of solar collector against the reduced temperature parameter for water and nanofluid at different concentrations and flow rates. It could be seen that as the value of  $\left(\frac{T_i - T_a}{G_T}\right)$  approaches to zero, the efficiency of the collector rises to its highest point because at this point the trend line intersects y-axis and the value of  $F_R(\tau\alpha)$  has become the maximum. The value of  $F_R U_L$  is obtained from the slope of the trend line. On the other hand, the point at which trend line intersects x-axis is called the stagnation point, and at this point the efficiency approaches zero and  $\left(\frac{T_i - T_a}{G_T}\right)$  is showing the maximum. At a particular value of reduced temperature parameter, utilizing nanofluid as an alternative of water at a higher value of heat flux and low value of input temperature the more useful performance is obtained according to the first law of thermodynamics [33].

As the reduced temperature parameter value increases, the efficiency line of water crosses the efficiency line of nanofluids at some point. The point of intersection of these efficiencies lines is called critical point, which represents that before the intersection of lines the efficiency of nanofluid is higher than that of water, but after intersection

point, water provides better output than nanofluid. Table 6 represents the values of the intersection point of the reduced temperature parameter against the different concentrations of CGNP.

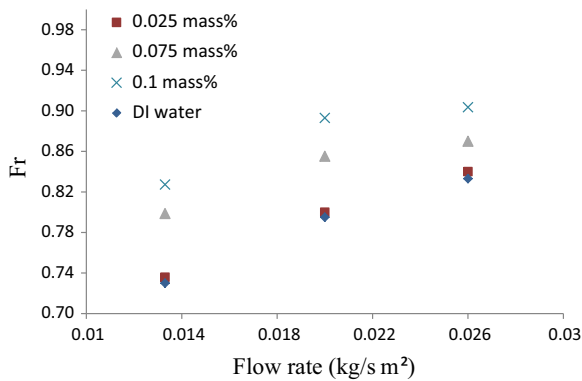
The heat removal factor  $F_R$  values are shown in Fig. 7. It was calculated using Eq. (7).

The results showed that heat removable factor for nanofluid is more than water. Also, it rises with the increasing mass flow rate. As the mass fraction of CGNP increases, the value of heat removable factor increases. Based on these results, the convective heat transfer coefficient was higher than that of water and both absorbed energy parameter  $F_R(\tau\alpha)$  and the removed energy parameter  $F_R U_L$  for CGNP nanofluid are increased. As a result of that, the performance of solar collector is enhanced when using CGNP–nanofluid.

Figure 8a–c represents the effect of mass fraction of CGNP on thermal performance of solar collector at mass fractions of 0.025, 0.075 and 0.1% and at several flow rates of 0.0133, 0.0200 and 0.026 kg s<sup>-1</sup> m<sup>-2</sup>. The thermal collector efficiency for CGNP against the reduced temperature parameter shows the mass fraction of nanoparticles has a significant effect on the thermal performance of solar collector. From Fig. 8a and Table 5, it is observed that at the flow rate of 0.0133 kg s<sup>-1</sup> m<sup>-2</sup> and concentrations of 0.025, 0.075 and 0.1 mass% the values of  $F_R(\tau\alpha)$  increased compared to water data by 5.42%, 19.67% and 21.51%, respectively, while the corresponding value of  $F_R U_L$  has increased by 12.40%, 15.70% and 24.57%. Based on Fig. 8b and Table 5, the enhancement in heat absorption factor and heat removal factor at the flow rate of 0.0200 kg s<sup>-1</sup> m<sup>-2</sup> at the mass fractions of CGNP 0.025, 0.75 and 0.1 mass% is 4.35, 18.56, 22.1 and 14.01, 18.57 and 21.82%, respectively, compared to water data at the same flow rate. Figure 8c and Table 5 represent that the improvement in  $F_R(\tau\alpha)$  is 4.87, 21.80 and 22.30% and  $F_R U_L$  is 16.75, 25.09 and 32.49% at the flow rate of

**Table 6** Intersection of CGNP nanofluids and the characteristics of water

Mass flow rate/kg s <sup>-1</sup> m <sup>-2</sup>	Mass concentration/mass%	Intersection (T <sub>i</sub> - T <sub>a</sub> )/G <sub>T</sub>
0.0133	0.1	0.058
	0.075	0.037
	0.025	0.036
0.0200	0.1	0.069
	0.075	0.035
	0.025	0.042
0.0260	0.1	0.055
	0.075	0.037
	0.025	0.046

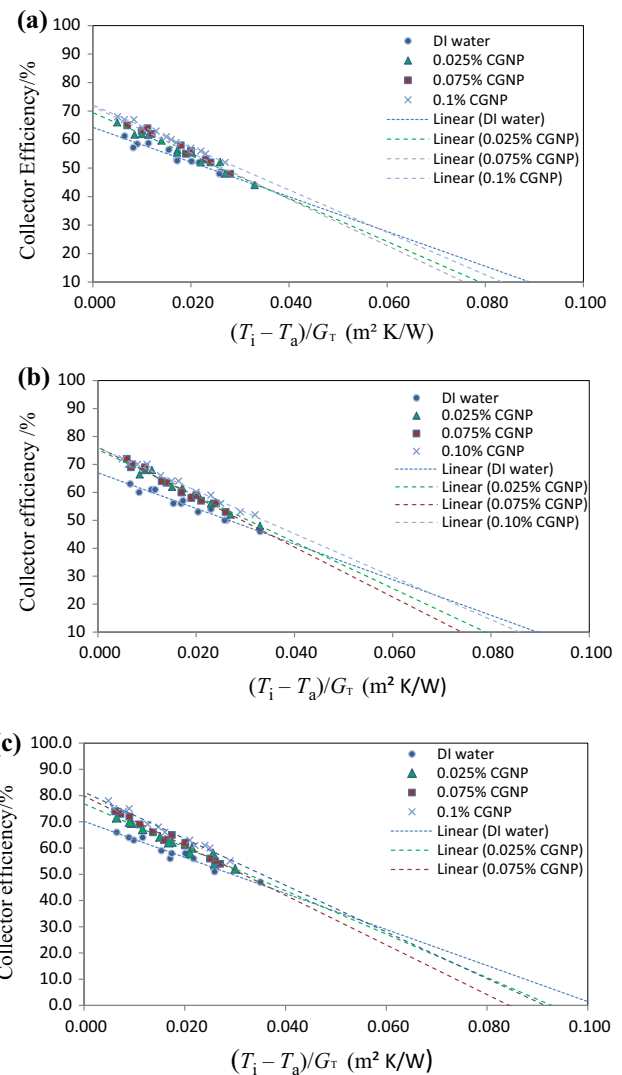
**Fig. 7** Heat removal factor at different flow rates and different mass concentrations

0.0260 kg s<sup>-1</sup> m<sup>-2</sup> at three concentrations of 0.025, 0.075 and 0.01 mass%, respectively.

It is observed from the aforementioned results that with the increment in mass fraction of nanoparticles, the value of heat absorption factor and the heat removal factor is increased. The highest value of  $F_R(\tau\alpha)$  and  $F_R U_L$  was observed at the flow rate of 0.0260 kg s<sup>-1</sup> m<sup>-2</sup>, and the efficiency of the collector was also found best at the same flow rate and at the higher concentration, i.e., 0.1 mass%.

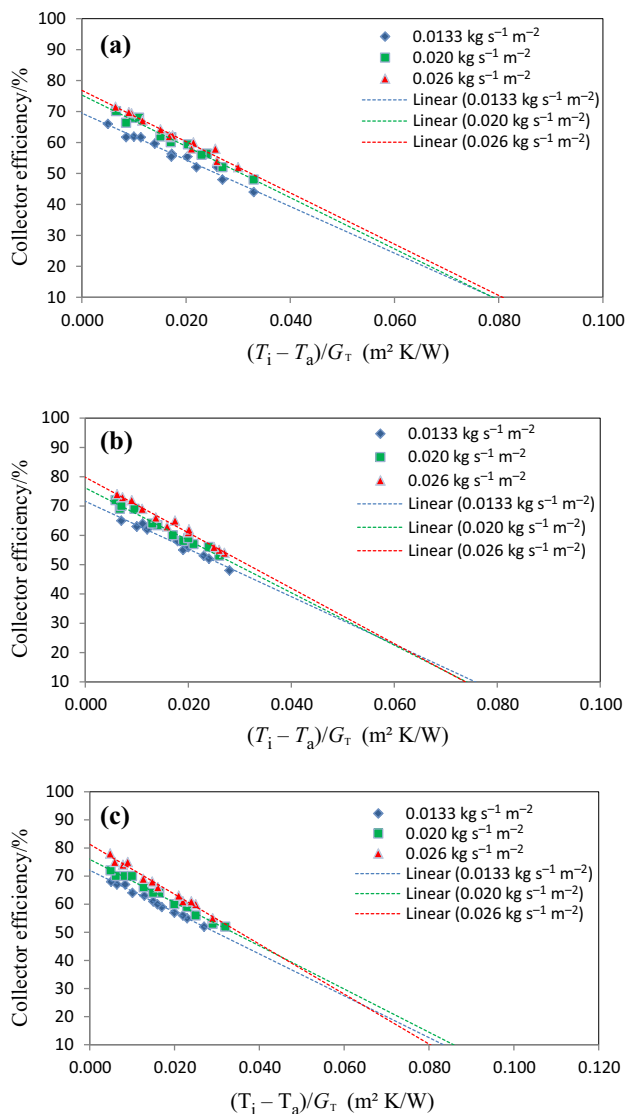
Mohsen Mirzaei et al [37]. found that the highest efficiency of Al<sub>2</sub>O<sub>3</sub>-water nanofluid is achieved for 2 L min<sup>-1</sup>, which increases the average of collector efficiency by 23.6% in comparison with that of pure water working fluid. The volume fraction of nanoparticles was set to 0.1% with the average particle size of 20 nm. M.A. Sharafeldin and Gyula Gróf [35] indicate that the highest rise in efficiency of the collector at zero value of  $[(T_i - T_a)/G_T]$  is 10.74%, for volume fraction ( $\phi$ ) 0.066% and for mass flux rate of 0.019 kg s<sup>-1</sup> m<sup>-2</sup> compared to water while in this study the highest thermal performance of solar collector could have reached 78% at mass concentration 0.1 mass% and flow rate 0.0260 kg s<sup>-1</sup> m<sup>-2</sup> which is 18.2% higher than water at the same flow rate conditions.

Figure 9a-c represents the thermal efficiency of solar collector against reduced temperature parameter at the

**Fig. 8** Thermal efficiency of FPSC at the flow rates **a** 0.0133, **b** 0.0200, **c** 0.0260 kg s<sup>-1</sup> m<sup>-2</sup>

concentration of CGNP 0.025, 0.075 and 0.1 mass% at the flow rates of 0.0133, 0.0200 and 0.0260 kg s<sup>-1</sup> m<sup>-2</sup>. As visualized in Fig. 9a-c, the thermal efficiency of solar collector increased with an increase in flow rate from

0.0133 to  $0.0260 \text{ kg s}^{-1} \text{ m}^{-2}$  at each of the concentrations. The maximum enhancement in thermal performance of solar collector in reduced temperature parameter was equal to 18.2%, at mass fraction 0.1 mass%, and the flow rate was kept at  $0.0260 \text{ kg s}^{-1} \text{ m}^{-2}$ . The value of  $F_R(\tau\alpha)$  and  $F_R U_L$  was noticed also gradual increase with the flow rate. This is because of the enhancement in Brownian motion, which also refers increase in Reynold number, Nusselt number and also improvement in the convective heat transfer coefficient [39].



**Fig. 9** Thermal efficiency of FPSC at the concentrations **a** 0.025, **b** 0.075, and **c** 0.1 mass%

## Conclusions

In this study, an experimental investigation was carried out for the first time, to document and articulate the effect of CGNP–water nanofluids for the enhancement of thermal efficiency of the FPSC. The stability of CGNP–water nanofluid was checked by zeta potential at different pH values. The CGNP–water nanofluids were found stable after 45 days, and no sedimentation was noticed. Three different mass fractions of nanoparticles such as 0.025, 0.075 and 0.01% were studied at three different mass flow rates  $0.0133$ ,  $0.0200$  and  $0.0260 \text{ kg s}^{-1} \text{ m}^{-2}$ . The outcomes elucidate that the addition of CGNP nanoparticles to water enriches the performance of FPSC, and the percentage of improvement in thermal performance depends on nanoparticle concentration, fluid mass flow rate and the inlet temperature which could cause to change the reduced temperature parameter. The highest thermal performance of a solar collector has reached 78% at a mass fraction of 0.1% and flow rate  $0.0260 \text{ kg s}^{-1} \text{ m}^{-2}$  which was 18.2% higher than water alone at the same conditions of reduced temperature parameter and flow rate. The maximum increment in the  $F_R(\tau\alpha)$  and  $F_R U_L$  was 22.30% and 26.79%, respectively, for the mass flow rate of  $0.0260 \text{ kg s}^{-1} \text{ m}^{-2}$  and particle concentration of 0.1 mass%.

**Acknowledgements** The first author would like to thank the Higher Education Commission of Pakistan (HEC) for their PhD Research Funding and Scholarship. Also, all the authors take an opportunity to acknowledge the High Impact Research Grant UMRG-RP045C-17AET and the University of Malaya, Malaysia, for the financial support in conducting the research work.

## References

1. Agency IAE, World Energy Outlook. Organization For Economic, S.I (2016), 2016.
2. BP Statistical Review of World Energy June 2016, B., 2016.
3. Shafiee S, Topal E. When will fossil fuel reserves be diminished? Energy Policy. 2009;37(1):181–9.
4. Rashidi S, et al. Applications of nanofluids in condensing and evaporating systems. J Therm Anal Calorim. 2018;131(3):207–39.
5. Mahian O, et al. Recent advances in modeling and simulation of nanofluid flows-part I: fundamental and theory 2018.
6. Mahian O, et al. Recent advances in modeling and simulation of nanofluid flows-part II: applications. 2018.
7. Amber K, et al. Heating and cooling degree-days maps of Pakistan. Energies. 2018;11(1):94.
8. Bellos E, Tzivanidis C, Calorimetry, A review of concentrating solar thermal collectors with and without nanofluids. 2018.
9. Natarajan E, Sathish R. Role of nanofluids in solar water heater. Int J Adv Manuf Technol. 2009. <https://doi.org/10.1007/s00170-008-1876-8>.

10. Bashirnezhad K, et al. A comprehensive review of last experimental studies on thermal conductivity of nanofluids. *J Therm Anal Calorim.* 2015;122(2):863–84.
11. Hosseini M, et al. Numerical study of turbulent heat transfer of nanofluids containing eco-friendly treated carbon nanotubes through a concentric annular heat exchanger. *Int J Heat Mass Transf.* 2018;127:403–12.
12. Sadri R, et al. CFD modeling of turbulent convection heat transfer of nanofluids containing green functionalized graphene nanoplatelets flowing in a horizontal tube: comparison with experimental data. *J Mol Liq.* 2018;269:152.
13. Sadri R, et al. Study of environmentally friendly and facile functionalization of graphene nanoplatelet and its application in convective heat transfer. *Energy Convers Manag.* 2017;150:26–36.
14. Choi SU, Eastman JA. Enhancing thermal conductivity of fluids with nanoparticles, 1995, Argonne National Lab., IL (United States).
15. Masuda H, Ebata A, Teramae K. Alteration of thermal conductivity and viscosity of liquid by dispersing ultra-fine particles. Dispersion of  $\text{Al}_2\text{O}_3$ ,  $\text{SiO}_2$  and  $\text{TiO}_2$  ultra-fine particles. *Netsu Bussei.* 1993;7(4):227–33.
16. Sundar LS, et al. Effectiveness analysis of solar flat plate collector with  $\text{Al}_2\text{O}_3$  water nanofluids and with longitudinal strip inserts. *Int J Heat Mass Transf.* 2018;127:422–35.
17. Yousefi T, et al. An experimental investigation on the effect of MWCNT- $\text{H}_2\text{O}$  nanofluid on the efficiency of flat-plate solar collectors. *Exp Therm Fluid Sci.* 2012;39:207–12.
18. Vijayakumar S, Shankar RL, Babu K. Effect of CNT-H 2 O nanofluid on the performance of solar flat plate collector—an experimental investigation. In: International conference on advanced nanomaterials and emerging engineering technologies (ICANMEET), 2013. IEEE.
19. Vakili M, et al. Experimental investigation of graphene nanoplatelets nanofluid-based volumetric solar collector for domestic hot water systems. *Sol Energy.* 2016;131:119–30.
20. Ahmadi A, Ganji DD, Jafarkazemi F. Analysis of utilizing Graphene nanoplatelets to enhance thermal performance of flat plate solar collectors. *Energy Convers Manag.* 2016;126:1–11.
21. Polvongsri S, Kiatsiriroat T. Enhancement of flat-plate solar collector thermal performance with silver nano-fluid. In: Second TSME international conference on mechanical engineering, Krabi, Thailand. 2011.
22. Yousefi T, et al. An experimental investigation on the effect of  $\text{Al}_2\text{O}_3$ - $\text{H}_2\text{O}$  nanofluid on the efficiency of flat-plate solar collectors. *Renew Energy.* 2012;39(1):293–8.
23. Jamal-Abad MT, et al. Experimental study of the performance of a flat-plate collector using Cu–water nanofluid. *J Thermophys Heat Transf.* 2013;27(4):756–60.
24. Said Z, et al. Experimental investigation of the thermophysical properties of  $\text{Al}_2\text{O}_3$ -nanofluid and its effect on a flat plate solar collector. *Int Commun Heat Mass Transf.* 2013;48:99–107.
25. Noghrehabadi A, Hajidavaloo E, Moravej M. Experimental investigation of efficiency of square flat-plate solar collector using  $\text{SiO}_2$ /water nanofluid. *Case Stud Therm Eng.* 2016;8:378–86.
26. Verma SK, Tiwari AK, Chauhan DS. Performance augmentation in flat plate solar collector using  $\text{MgO}$ /water nanofluid. *Energy Convers Manag.* 2016;124:607–17.
27. Vincely DA, Natarajan E. Experimental investigation of the solar FPC performance using graphene oxide nanofluid under forced circulation. *Energy Convers Manag.* 2016;117:1–11.
28. Said Z, et al. Energy and exergy efficiency of a flat plate solar collector using pH treated  $\text{Al}_2\text{O}_3$  nanofluid. *J Clean Prod.* 2016;112:3915–26.
29. Kim H, Kim J, Cho H. Experimental study on performance improvement of U-tube solar collector depending on nanoparticle size and concentration of  $\text{Al}_2\text{O}_3$  nanofluid. *Energy.* 2017;118:1304–12.
30. Jouybari HJ, et al. Effects of porous material and nanoparticles on the thermal performance of a flat plate solar collector: an experimental study. *Renew Energy.* 2017;114:1407–18.
31. Sharafeldin MA, Gróf G, Mahian O. Experimental study on the performance of a flat-plate collector using  $\text{WO}_3$ /Water nanofluids. *Energy.* 2017;141:2436–44.
32. Kang W, Shin Y, Cho H. Economic Analysis of Flat-Plate and U-Tube Solar Collectors Using an  $\text{Al}_2\text{O}_3$  Nanofluid. *Energies.* 2017;10(11):1911.
33. Stalin PMJ, et al. Experimental and theoretical investigation on the effects of lower concentration  $\text{CeO}_2$ /water nanofluid in flat-plate solar collector. *J Therm Anal Calorim.* 135(1):29–44.
34. Sundar LS, et al. Experimental investigation of  $\text{Al}_2\text{O}_3$ /water nanofluids on the effectiveness of solar flat-plate collectors with and without twisted tape inserts. *Renew Energy.* 2018;119:820–33.
35. Sharafeldin M, Gróf G. Experimental investigation of flat plate solar collector using  $\text{CeO}_2$ -water nanofluid. *Energy Convers Manag.* 2018;155:32–41.
36. Farajzadeh E, Movahed S, Hosseini R. Experimental and numerical investigations on the effect of  $\text{Al}_2\text{O}_3/\text{TiO}_2/\text{H}_2\text{O}$  nanofluids on thermal efficiency of the flat plate solar collector. *Renew Energy.* 2018;118:122–30.
37. Mirzaei M, Hosseini SMS, Kashkooli AMM. Assessment of  $\text{Al}_2\text{O}_3$  nanoparticles for the optimal operation of the flat plate solar collector. *Appl Therm Eng.* 2018;134:68–77.
38. Verma SK, Tiwari AK, Chauhan DS. Experimental evaluation of flat plate solar collector using nanofluids. *Energy Convers Manag.* 2017;134:103–15.
39. Sadri R, et al. A facile, bio-based, novel approach for synthesis of covalently functionalized graphene nanoplatelet nano-coolants toward improved thermo-physical and heat transfer properties. *J Colloid Interface Sci.* 2018;509:140–52.
40. Aravind SJ, et al. Investigation of structural stability, dispersion, viscosity, and conductive heat transfer properties of functionalized carbon nanotube based nanofluids. *J Phys Chem C.* 2011;115(34):16737–44.
41. Sadri R, et al. A bio-based, facile approach for the preparation of covalently functionalized carbon nanotubes aqueous suspensions and their potential as heat transfer fluids. *J Colloid Interface Sci.* 2017;504:115–23.
42. Mahian O, et al. A review of the applications of nanofluids in solar energy. *Int J Heat Mass Transf.* 2013;57(2):582–94.
43. Yu W, Xie H. A review on nanofluids: preparation, stability mechanisms, and applications. *J Nanomater.* 2012;2012:1.
44. Soudagar MEM, et al. The effect of nano-additives in diesel-biodiesel fuel blends: a comprehensive review on stability, engine performance and emission characteristics. *Energy Convers Manag.* 2018;178:146–77.
45. Standard A, Standard 93-2003. Method of testing to determine the thermal performance of solar collector, 2003.
46. Duffie JA, Beckman WA. Solar engineering of thermal processes. Hoboken: Wiley; 2013.
47. Pak BC, Cho YI. Hydrodynamic and heat transfer study of dispersed fluids with submicron metallic oxide particles. *Exp Heat Transf.* 1998;11(2):151–70.
48. Montazer E, et al. Development of a new density correlation for carbon-based nanofluids using response surface methodology. *J Therm Anal Calorim.* 2018;132(2):1399–407.
49. Zhang X, et al. Effective thermal conductivity and thermal diffusivity of nanofluids containing spherical and cylindrical nanoparticles. *Exp Therm Fluid Sci.* 2007;31(6):593–9.

50. Srivastva U, et al. Review of heat transport properties of solar heat transfer fluids. *J Therm Anal Calorim.* 2017;130(2):605–21.
51. Holman JP. *Experimental methods for engineers.* 8th ed. New York: McGraw-Hill; 2012.
52. Kline SJJME. Describing uncertainty in single sample experiments. *Mech Eng.* 1953;75:3–8.
53. Alawi OA, et al. Thermophysical properties and stability of carbon nanostructures and metallic oxides nanofluids. *J Therm Anal Calorim.* 2018;135(2):1545–62.
54. Chon C, Kihm KD. Thermal conductivity enhancement of nanofluids by Brownian motion. *J Heat Transf-Trans ASME.* 2005;127(8):810.

**Publisher's Note** Springer Nature remains neutral with regard to jurisdictional claims in published maps and institutional affiliations.